Journal of Applied Electrochemistry (2020) 50:63–69
https://doi.org/10.1007/s10800-019-01369-0

RESEARCH ARTICLE

Plasmon-enhanced hierarchical photoelectrodes with mechanical flexibility for hydrogen generation from urea solution and human urine

Jiayong Gan[1] · **Bharath Bangalore Rajeeva**[1] · **Zilong Wu**[1] · **Daniel Penley**[1] · **Yuebing Zheng**[1]

Received: 4 July 2019 / Accepted: 24 October 2019 / Published online: 6 November 2019

Abstract

We have demonstrated plasmon-enhanced flexible and hierarchical photoanodes for hydrogen production from human urine in a photoelectrochemical cell. The photoanodes consist of cobalt-doped α-Fe_2O_3 nanorod arrays functionalized with Au nanoparticles and $Ni(OH)_2$. The Au nanoparticles and $Ni(OH)_2$ work as plasmonic nanostructures and urea oxidation catalyst, respectively. Benefiting from the plasmonic and catalytic effects, the photoanodes exhibit an AM 1.5 photocurrent of 5.0 ± 0.1 mA cm^{-2} (urea solution) and 7.5 ± 0.1 mA cm^{-2} (human urine) at 0.3 V versus Ag/AgCl. At a Pt counter electrode, continuous hydrogen gas evolution is achieved at a small bias. With their high performance and mechanical flexibility that facilitates the large-scale transportation and implementation in the field, the photoanodes are paving a sustainable way towards hydrogen production and urine treatment.

Graphic abstract

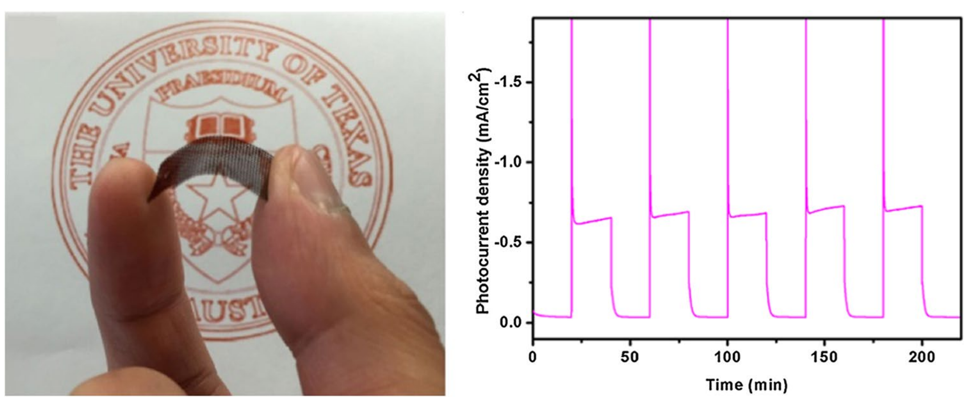

Keywords Flexible photoelectrode · Hydrogen production · Photoelectrochemical cell · Urine · Plasmonic effects

1 Introduction

Sustainable hydrogen supply could help solve many energy challenges [1–8]. Despite being promising hydrogen sources, hydrazine and metal hydrides suffer from high cost, toxicity, flammability, and limited quantity [6]. Urea [$CO(NH_2)_2$] was proposed as an alternative hydrogen source for its high hydrogen content (6.71%), abundance, low cost, and non-flammability [6, 9, 10]. Millions of tons of human and animal urine produced on a daily

Electronic supplementary material The online version of this article (https://doi.org/10.1007/s10800-019-01369-0) contains supplementary material, which is available to authorized users.

✉ Yuebing Zheng
zheng@austin.utexas.edu

[1] Walker Department of Mechanical Engineering, Materials Science and Engineering Program, Texas Materials Institute, The University of Texas at Austin, Austin, TX 78712, USA

basis, which adversely impacts the environment, has a concentration of urea ranging from 0.155 to 0.39 mole/L [11]. Therefore, it benefits both energy and the environment to generate hydrogen from urine.

There are multiple approaches for hydrogen production from urea. One technique involves urea decomposition and high-temperature cracking of ammonia, which is energy-intensive with safety issue [12]. Another technique employs an external bias and a urea oxidation catalyst to electrolyze aqueous urea solution for hydrogen, which consumes a substantial amount of electricity [11, 13–17]. A more sustainable technique for hydrogen generation from urea in human urine is driven by solar cells that power an electrolyzer for urea electrolysis. Alternatively, a high-performance and portable photoelectrochemical (PEC) cell is promising for cost-effective hydrogen production from human and animal urine.

Herein, we have developed mechanically flexible plasmon-enhanced photoanodes of hierarchical architectures for portable PEC cells that enable solar-driven efficient hydrogen generation from human and animal urine in the field. The anodes are based on cobalt-doped Fe_2O_3 nanorod arrays (Co–Fe_2O_3 NRAs) on flexible Ti mesh substrates. α-Fe_2O_3 and its variants are promising semiconductors for PEC cells because of their high stability, abundance, and low cost [18–21]. The Co–Fe_2O_3 NRAs on Ti mesh substrates feature a large surface–volume ratio for enhanced photochemical reaction efficiency along with a strong mechanical flexibility for the large-scale implementation [22]. We further functionalize the NRAs with plasmonic Au nanoparticles (NPs) and $Ni(OH)_2$ as urea oxidation catalyst to create the composite photoanodes, which are indicated as $Ni(OH)_2$/Au@Co–Fe_2O_3 NRAs. Due to their nanoscale concentration and enhancement of electromagnetic fields, plasmonic nanostructures have been employed to improve non-linear optics [23, 24], biosensors [25], and energy devices [26]. In particular, the use of plasmonic nanostructures to enhance solar energy conversion and storage has attracted strong interests [27–29]. We aim to harness the plasmonic effects and their associated phenomena such as hot carrier injection, resonance energy transfer, and plasmonic heating to enhance photochemical reactions in PEC cells [30–34].

With the synergistic effects of hierarchical structures, plasmonic effects, and catalysis, our composite photoanodes exhibit high-performance solar-driven PEC hydrogen production from urea and human urine at a small external bias. The flexible photoanodes can be folded into a compact form for the large-scale transportation and implementation in the field, paving the way towards sustainable hydrogen production and urine treatment for environmental protection.

2 Results and discussions

We synthesized Co–Fe_2O_3 NRAs on flexible Ti mesh substrates using hydrothermal method (see Supporting Information) [35]. X-ray diffraction studies confirm that the NRAs have a Rhombohedral Hematite structure (JCPDS 1-1053) (Fig. S1). Next, Au NPs were deposited on the NRAs by sputtering and thermal annealing to create Au@Co–Fe_2O_3 NRAs (see Supporting Information). The mechanical flexibility of Ti mesh substrates was retained after the formation of NRAs and Au NPs (Fig. 1a). As shown in Figs. 1b and c, highly dense and uniform Co–Fe_2O_3 NRAs were formed perpendicular to the surfaces of Ti wires of the mesh. The NRAs grew radially outward around the entire surfaces of the Ti wires to form branched three-dimensional (3D) structures with a large surface–volume ratio. To promote urea oxidation kinetics, we utilized a dip-coating method to deposit $Ni(OH)_2$ as an electrochemical catalyst on the Au@Co–Fe_2O_3 NRAs, completing synthesis of composite photoanodes indicated as $Ni(OH)_2$/Au@Co–Fe_2O_3 NRAs. In Fig. 1d, transmission electron micrograph (TEM) of $Ni(OH)_2$/Au@Co–Fe_2O_3 NRAs reveals the amorphous nature of $Ni(OH)_2$ on the photoanodes. The lattice fringe with a spacing of 0.3775 nm agrees with (012) plane of Co–Fe_2O_3 nanorods (JCPDS 1-1053). Energy-dispersive X-ray spectroscopy (EDS) confirms the presence of Ni on Au@Co–Fe_2O_3 NRAs (Fig. S2). The atomic percentage of Ni was determined to be ~ 1.8% according to the EDS result. The percentage of $Ni(OH)_2$ is therefore ~ 9%.

We evaluated the light absorption properties of Co–Fe_2O_3, $Ni(OH)_2$@Co–Fe_2O_3, and $Ni(OH)_2$/Au@Co–Fe_2O_3 NRAs using diffused reflectance UV–visible spectroscopy. As shown in Fig. 2a, Co–Fe_2O_3 NRAs absorb light at wavelengths that are shorter than 580 nm, corresponding to electronic band gap of Fe_2O_3 (i.e., 2.2 eV). The absorption edge of Co–Fe_2O_3 NRAs does not exhibit a significant change after the $Ni(OH)_2$ functionalization. In contrast, $Ni(OH)_2$/Au@Co–Fe_2O_3 NRAs exhibit an additional absorption at wavelengths from 510 to 575 nm, which arises from the excitation of localized surface plasmon resonances (LSPRs) of Au NPs [36]. The plasmonic effects lead to the enhanced PEC performance of $Ni(OH)_2$/Au@Co–Fe_2O_3 NRAs as discussed below.

We comparatively studied the PEC performance of Co–Fe_2O_3, Au@Co–Fe_2O_3, and $Ni(OH)_2$/Au@Co–Fe_2O_3 NRAs for urea oxidation under solar-simulated illumination (AM 1.5, 100 mW cm^{-2}). Both commercial urea solution and human urine were used. Figures 2b–d are the experimental results for the urea solution. Figure 2b shows that, under light illumination, Co–Fe_2O_3 and Au@Co–Fe_2O_3 NRAs have the onset potential for urea

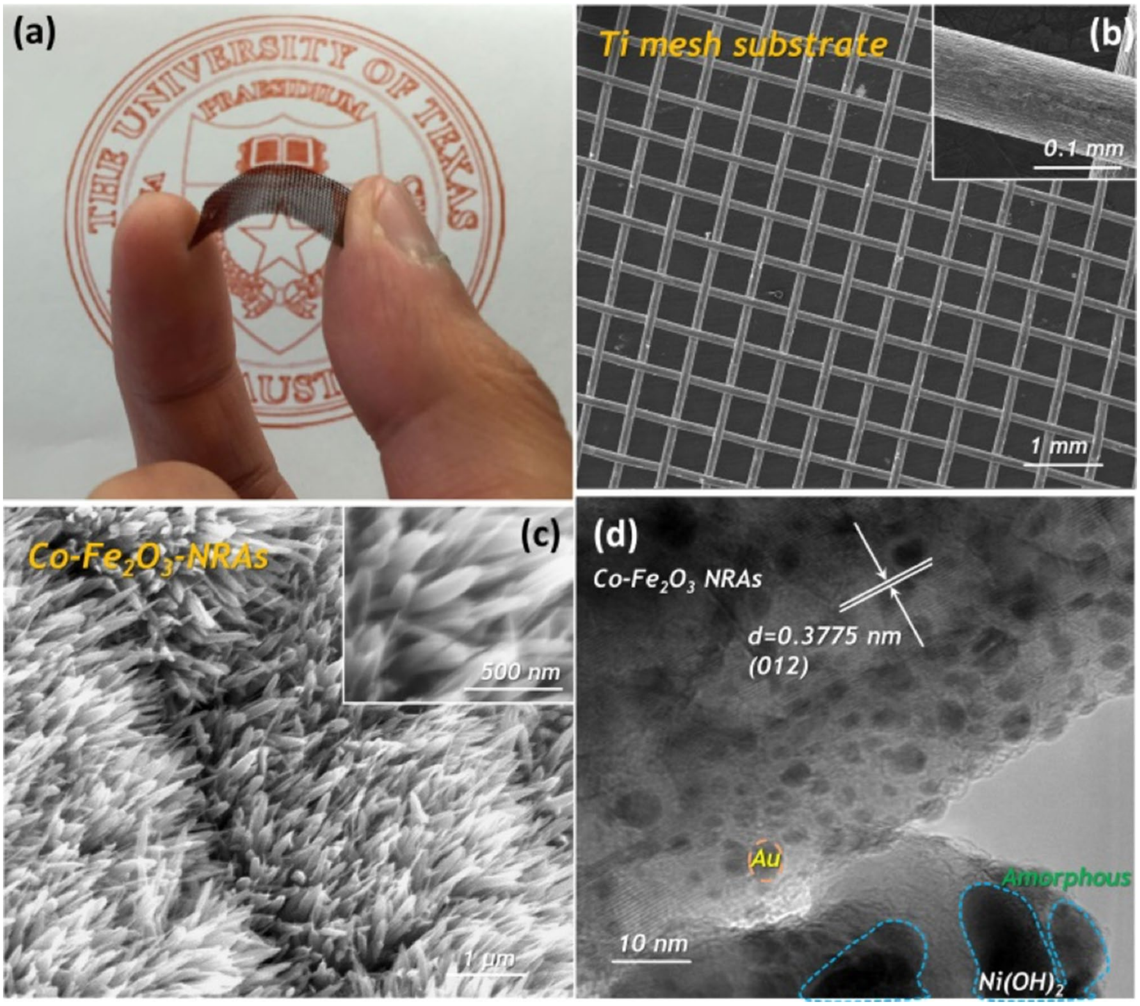

Fig. 1 **a** Photograph of a flexible Ti mesh consisted of $Ni(OH)_2$/Au@Co–Fe_2O_3 NRAs as photoanodes. **b** Scanning electron microscopic (SEM) image of the Ti mesh. **c** SEM image of Co–Fe_2O_3 NRAs on the Ti mesh. **d** Transmission electron micrograph of $Ni(OH)_2$/Au@Co–Fe_2O_3 NRAs

oxidation shifted to − 0.2 V versus Ag/AgCl. However, theoretical potential for urea electrolysis is 0.35 V versus Ag/AgCl [13]. The potential reduction can be attributed to urea oxidation driven by photovoltage in Co–Fe_2O_3. Compared with Co–Fe_2O_3, Au@Co–Fe_2O_3 yielded an enhanced anodic photocurrent of up to 2.8 mA cm^{-2} at 0.35 V versus Ag/AgCl, suggesting the plasmonic enhancement from the Au NPs. $Ni(OH)_2$/Au@Co–Fe_2O_3 NRAs exhibit the lower onset potential and substantially higher photocurrent than Co–Fe_2O_3 and Au@Co–Fe_2O_3. It is envisaged that, in the $Ni(OH)_2$/Au@Co–Fe_2O_3 NRAs, the photoexcited holes in Co–Fe_2O_3 can oxidize $Ni(OH)_2$ to NiOOH, which further catalyzes the urea oxidation with a reduced electrode overpotential [37]. Meanwhile, the photoexcited electrons can be transferred to a Pt counter electrode to reduce water to hydrogen gas. We observed continuous gas evolution on the Pt wire under light illumination, as shown in Video S1.

The photoelectrochemical oxidation of urine involves H_2O and $CO(NH_2)_2$, which are major components among the 3079 types of chemical species in human urine [38]. Upon light illumination, the following chemical processes occur on the cathodes and anodes.

Cathode:

$$Fe_2O_3 + h\nu \rightarrow Fe_2O_3^* + e^- + h^+$$
$$Ni(OH)_2 + OH^- + h^+ \rightarrow NiOOH + H_2O$$
$$6NiOOH + CO(NH_2)_2 + H_2O \rightarrow 6Ni(OH)_2 + CO_2 + N_2$$

Anode:

$$2H_2O + 2e^- \rightarrow H_2 + 2OH^-.$$

The total chemical processes can be summarized as

$$CO(NH_2)_2 + H_2O \rightarrow 3H_2 + CO_2 + N_2.$$

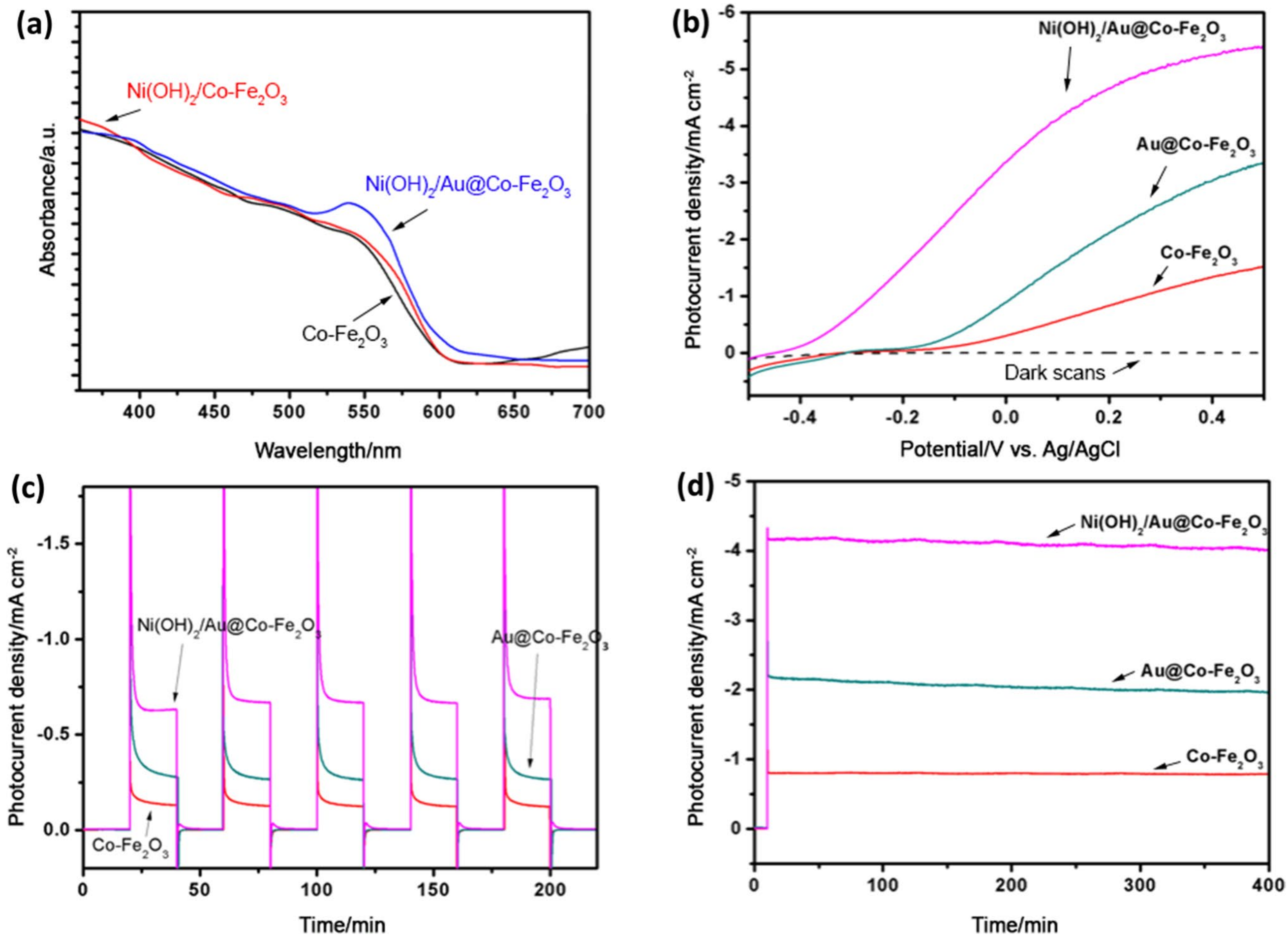

Fig. 2 **a** Optical absorption spectra of Co–Fe_2O_3, $Ni(OH)_2$@Co–Fe_2O_3, and $Ni(OH)_2$/Au@Co–Fe_2O_3 NRAs as photoanodes. **b** Linear sweep voltammograms collected for the three types of photoanodes in a 1.0 M NaOH aqueous solution in the presence of 0.33 M urea in the dark (dashed lines indicated by "dark scans") and under AM 1.5G illumination (100 mW cm^{-2}). **c** Photocurrent–time response curves of the three types of photoanodes collected at a zero bias in a two-electrode electrochemical cell under chopped AM 1.5G illumination (100 mW cm^{-2}). **d** Photocurrent–time response curves of the three types of photoanodes collected at 0.2 V versus Ag/AgCl under chopped AM 1.5G illumination (100 mW cm^{-2})

Therefore, the final products of the photoelectrochemical oxidation are non-toxic gaseous molecules that are not harmful to the environment.

Figure 2c shows the photocurrent density–time response curves measured for the three types of photoanodes at a zero bias. We made the measurements using a two-electrode electrochemical cell under chopped AM 1.5 G illumination (100 mW cm^{-2}). Stable photocurrent densities of 0.15 mA cm^{-2}, 0.30 mA cm^{-2}, and 0.65 mA cm^{-2} were achieved for Co–Fe_2O_3, Au@Co–Fe_2O_3, and $Ni(OH)_2$/Au@Co–Fe_2O_3 NRAs, respectively. Therefore, the synergy of LSPRs at AuNPs and urea oxidation catalysis of $Ni(OH)_2$ can significantly enhance the performance of solar-driven urea oxidation and hydrogen production at small or zero external bias. The photocurrent transient was observed under zero bias, for the reason that the charge was not effectively separated at the interface of the electrolyte and Au@Co–Fe_2O_3. We also conducted the long-term stability test at 0.2 V versus Ag/AgCl for solar-driven urea oxidation. No apparent photocurrent density decay was detected for at least 400 min in all the samples, implying the sustainability for long-term operation of plasmonic enhanced PEC solar-driven urea oxidation.

Encouraged by the performance of solar-driven urea oxidation, we further employed the optimized $Ni(OH)_2$/Au@Co–Fe_2O_3 electrodes for solar-driven oxidation of urea in human urine. The linear sweep voltammogram measured under dark conditions for $Ni(OH)_2$/Au@Co–Fe_2O_3 NRAs exhibited a similar onset potential in urine and urea electrolyte solutions. A lower onset potential of − 0.42 V versus Ag/AgCl was observed under light illumination (Fig. 3a). The urine samples generated a higher current than the urea sample at 0.35 V versus Ag/AgCl due to the diversity of urea and metabolites in urine solution. The inorganic and

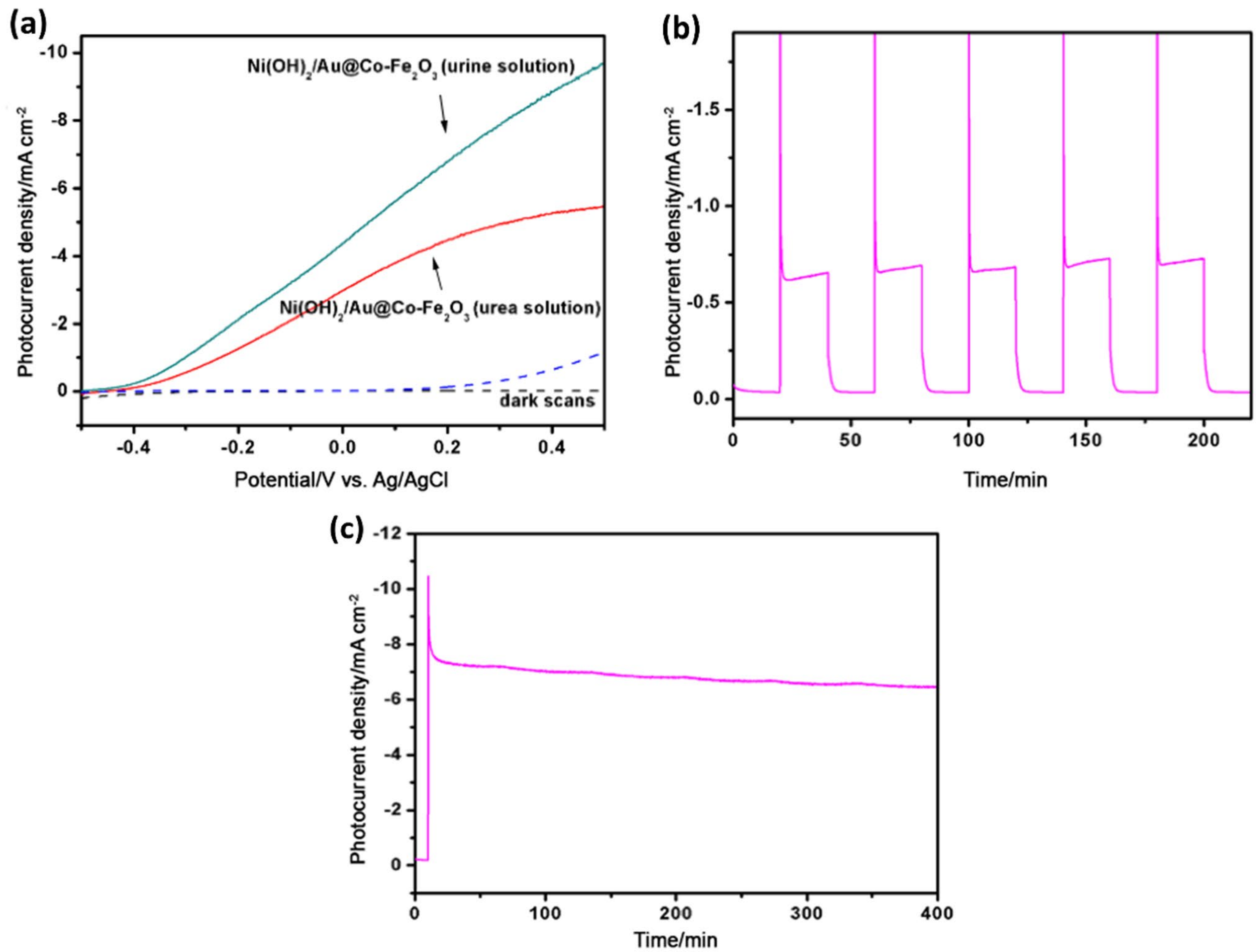

Fig. 3 **a** Linear sweep voltammograms collected for the $Ni(OH)_2$/Au@Co–Fe_2O_3 NRAs as a photoanode in a urea electrolyte solution and a human urine electrolyte solution in the dark (dashed lines by "dark scans") and under AM 1.5G illumination (100 mW cm^{-2}). **b** Photocurrent–time response curve of the $Ni(OH)_2$/Au@Co–Fe_2O_3 NRAs as a photoanode collected at a zero bias in a two-electrode electrochemical cell in human urine solution under chopped AM 1.5G illumination (100 mW cm^{-2}). **c** Photocurrent–time response curve of the $Ni(OH)_2$/Au@Co–Fe_2O_3 NRAs as a photoanode collected at 0.2 V versus Ag/AgCl under the same condition of (**b**)

organic metabolites in human urine also contribute to increment in the current. The photocurrent density–time response curve collected for the electrode in urine solution at zero bias under chopped light illumination exhibited a photocurrent density of 0.68 mA cm^{-2} (Fig. 3b). The performance at a zero bias substantiates the applicability of plasmon-enhanced urea photooxidation for practical applications in unassisted devices. In addition, the electrode showed stable photocurrent density in urine solution for at least 400 min (Fig. 3c), along with continuous hydrogen gas evolution at the Pt wire counter electrode at 0.2 V versus Ag/AgCl (Video S2). The successful demonstration of the flexible $Ni(OH)_2$/Au@Co–Fe_2O_3 NRAs for solar-driven hydrogen evolution from human urine provides a new opportunity for sustainable hydrogen generation and biological waste treatment.

We attribute the improved PEC performance to multiple enhancement mechanisms occurring in the composite photoelectrodes. When the optical absorption of Co–Fe_2O_3 overlaps with the LSPRs of the Au NPs, the near-field electromagnetic localization and enhancements improve the light absorption and facilitate the generation of electron–hole pairs. Further, the non-radiative decay of the LSPRs on Au NPs can generate plasmon-induced hot electrons and holes. The hot electrons were injected into the conduction band of Fe_2O_3, and eventually migrate to the cathode, where they interact with urine to form hydrogen under small amount of bias. Simultaneously, the hot holes and the photoexcited holes from Co–Fe_2O_3 oxidize $Ni(OH)_2$ to NiOOH, a well-known electrochemical catalyst for urea oxidization that produces N_2 and CO_2 [13, 14]. The photoexcited electrons from Co–Fe_2O_3 can reduce urine at the counter electrode as well.

Lastly, plasmon resonance energy transfer also contributes to the carrier generation in Co–Fe_2O_3.

3 Conclusions

Mechanically flexible and hierarchical photoanodes of Co–Fe_2O_3 NRAs with plasmonic enhancement and catalysis enable efficient hydrogen production from urea and human urine. We attribute the enhanced PEC performances of the composite photoanodes to the combined plasmonic effects of Au NPs and catalytic effects of $Ni(OH)_2$ along with the hierarchical nanoarchitectures. The mechanical flexibility of the photoelectrodes facilitates the effective transportation and implementation of the PEC cells for the sustainable production of renewable energy from wastewater.

Acknowledgements The authors acknowledge the financial support of the National Science Foundation (CBET-1704634).

References

1. Stewart SM, Spernjak D, Borup R, Datye A, Garzon F (2014) Cerium migration through hydrogen fuel cells during accelerated stress testing. ECS Electrochem Lett 3(4):F19–F22
2. Gao F, Zhao GL, Yang SZ (2014) Catalytic reactions on the open-edge sites of nitrogen-doped carbon nanotubes as cathode catalyst for hydrogen fuel cells. ACS Catal 4(5):1267–1273
3. Bardhan R, Ruminski AM, Brand A, Urban JJ (2011) Magnesium nanocrystal-polymer composites: a new platform for designer hydrogen storage materials. Energy Environ Sci 4(12):4882–4895
4. Lu YZ, Jin RT, Chen W (2011) Highly efficient hydrogen storage with PDAG nanotubes. Nanoscale 3(6):2476–2480
5. Parrondo J, Han T, Niangar E, Wang C, Dale N, Adjemian K, Ramani V (2014) Platinum supported on titanium-ruthenium oxide is a remarkably stable electrocatayst for hydrogen fuel cell vehicles. Proc Natl Acad Sci USA 111(1):45–50
6. Rollinson AN, Jones J, Dupont V, Twigg MV (2011) Urea as a hydrogen carrier: a perspective on its potential for safe, sustainable and long-term energy supply. Energy Environ Sci 4(4):1216–1224
7. Asghar A, Raman AA, Daud WMW (2015) Challenges and recommendations for using membranes in wastewater-based microbial fuel cells for in situ fenton oxidation for textile wastewater treatment. Rev Chem Eng 31(1):45–67
8. Mehmood A, Ha HY (2014) Performance restoration of direct methanol fuel cells in long-term operation using a hydrogen evolution method. Appl Energy 114:164–171
9. Shaegh SAM, Ehteshami SMM, Chan SH, Nguyen NT, Tan SN (2014) Membraneless hydrogen peroxide micro semi-fuel cell for portable applications. RSC Adv 4(70):37284–37287
10. Wang GM, Ling YC, Lu XH, Wang HY, Qian F, Tong YX, Li Y (2012) Solar driven hydrogen releasing from urea and human urine. Energy Environ Sci 5(8):8215–8219
11. Boggs BK, King RL, Botte GG (2009) Urea electrolysis: direct hydrogen production from urine. Chem Commun 32:4859–4861
12. Thomas G, Parks G (2006) Potential roles of ammonia in a hydrogen economy: a study of issues related to the use ammonia for on-board vehicular hydrogen storage. US Department of Energy, February
13. Yan W, Wang D, Diaz LA, Botte GG (2014) Nickel nanowires as effective catalysts for urea electro-oxidation. Electrochim Acta 134:266–271
14. Ding R, Qi L, Jia MJ, Wang HY (2014) Facile synthesis of mesoporous spinel $NiCo_2O_4$ nanostructures as highly efficient electrocatalysts for urea electro-oxidation. Nanoscale 6(3):1369–1376
15. Wang L, Du TT, Cheng J, Xie X, Yang BL, Li MT (2015) Enhanced activity of urea electrooxidation on nickel catalysts supported on tungsten carbides/carbon nanotubes. J Power Sources 280:550–554
16. Vedharathinam V, Botte GG (2014) Experimental investigation of potential oscillations during the electrocatalytic oxidation of urea on Ni catalyst in alkaline medium. J Phys Chem C 118(38):21806–21812
17. Wu MS, Lin GW, Yang RS (2014) Hydrothermal growth of vertically-aligned ordered mesoporous nickel oxide nanosheets on three-dimensional nickel framework for electrocatalytic oxidation of urea in alkaline medium. J Power Sources 272:711–718
18. Zhong DK, Sun JW, Inumaru H, Gamelin DR (2009) Solar water oxidation by composite catalyst/alpha-Fe_2O_3 photoanodes. J Am Chem Soc 131(17):6086–6087
19. Hou Y, Zuo F, Dagg A, Feng PY (2012) Visible light-driven alpha-fe_2o_3nanorod/graphene/Biv1-Xmoxo4 core/shell heterojunction array for efficient photoelectrochemical water splitting. Nano Lett 12(12):6464–6473
20. Segev G, Dotan H, Malviya KD, Kay A, Mayer MT, Gratzel M, Rothschild A (2016) High solar flux concentration water splitting with hematite (alpha-Fe_2O_3) photoanodes. Adv Energy Mater. https://doi.org/10.1002/aenm.201500817
21. Celorrio V, Bradley K, Weber OJ, Hall SR, Fermin DJ (2014) Photoelectrochemical properties of $LaFeO_3$ nanoparticles. ChemElectroChem 1(10):1667–1671
22. Wei YF, Ke L, Kong JH, Liu H, Jiao ZH, Lu XH, Du HJ, Sun XW (2012) Enhanced photoelectrochemical water-splitting effect with a bent ZnO nanorod photoanode decorated with Ag nanoparticles. Nanotechnology. https://doi.org/10.1088/0957-4484/23/23/235401
23. Liu YM, Zhang X (2011) Metamaterials: a new frontier of science and technology. Chem Soc Rev 40(5):2494–2507
24. Rajeeva BB, Hernandez DS, Wang M, Perillo E, Lin L, Scarabelli L, Pingali B, Liz-Marzán LM, Dunn AK, Shear JB (2015) Regioselective localization and tracking of biomolecules on single gold nanoparticles. Adv Sci 2(11):1500232
25. Lin LH, Zheng YB (2015) Engineering of parallel plasmonic-photonic interactions for on-chip refractive index sensors. Nanoscale 7(28):12205–12214
26. Boriskina SV, Ghasemi H, Chen G (2013) Plasmonic materials for energy: from physics to applications. Mater Today 16(10):375–386
27. Warren SC, Thimsen E (2012) Plasmonic solar water splitting. Energy Environ Sci 5(1):5133–5146
28. Catchpole KR, Polman A (2008) Plasmonic solar cells. Opt Express 16(26):21793–21800
29. Christopher P, Xin HL, Linic S (2011) Visible-light-enhanced catalytic oxidation reactions on plasmonic silver nanostructures. Nat Chem 3(6):467–472
30. Zhang TT, Zhao HY, He SN, Liu K, Liu HY, Yin YD, Gao CB (2014) Unconventional route to encapsulated ultrasmall gold nanoparticles for high-temperature catalysis. ACS Nano 8(7):7297–7304
31. Mubeen S, Lee J, Liu DY, Stucky GD, Moskovits M (2015) Panchromatic photoproduction of H-2 with surface plasmons. Nano Lett 15(3):2132–2136
32. Ranasingha OK, Wang CJ, Ohodnicki PR, Lekse JW, Lewis JP, Matranga C (2015) Synthesis, characterization, and

photocatalytic activity of Au-Zno nanopyramids. J Mater Chem A 3(29):15141–15147
33. Gao HW, Liu C, Jeong HE, Yang PD (2012) Plasmon-enhanced photocatalytic activity of iron oxide on gold nanopillars. ACS Nano 6(1):234–240
34. Liu ZW, Hou WB, Pavaskar P, Aykol M, Cronin SB (2011) Plasmon resonant enhancement of photocatalytic water splitting under visible illumination. Nano Lett 11(3):1111–1116
35. Hou Y, Zuo F, Dagg A, Feng PY (2013) A Three-dimensional branched cobalt-doped alpha-Fe_2O_3 nanorod/$MgFe_2O_4$ heterojunction array as a flexible photoanode for efficient photoelectrochemical water oxidation. Angew Chem Int Ed 52(4):1248–1252
36. Zhao J, Pinchuk AO, Mcmahon JM, Li SZ, Ausman LK, Atkinson AL, Schatz GC (2008) Methods for describing the electromagnetic properties of silver and gold nanoparticles. Acc Chem Res 41(12):1710–1720
37. Xu DD, Fu ZW, Wang DJ, Lin YH, Sun YJ, Meng DD, Xie TF (2015) A Ni(Oh)(2)-modified Ti-doped alpha-Fe_2O_3 photoanode for improved photoelectrochemical oxidation of urea: the role of Ni(Oh)(2) as a Co catalyst. Phys Chem Chem Phys 17(37):23924–23930
38. Bouatra S, Aziat F, Mandal R, Guo AC, Wilson MR, Knox C, Bjorndahl TC, Krishnamurthy R, Saleem F, Liu P (2013) The human urine metabolome. PLoS ONE 8(9):e73076